Electrochimica Acta 173 (2015) 377–384

Contents lists available at ScienceDirect

Electrochimica Acta

journal homepage: www.elsevier.com/locate/electacta

High performance electrode materials for electric double-layer capacitors based on biomass-derived activated carbons

Dabin Wang [a,b], Zhen Geng [a,c], Bing Li [a,b], Cunman Zhang [a,b,*]

[a] Clean Energy Automotive Engineering Center, Tongji University, Shanghai 201804, China
[b] School of Automotive Studies, Tongji University, Shanghai 201804, China
[c] School of Materials Science and Technology, Tongji University, Shanghai 201804, China

ARTICLE INFO

Article history:
Received 3 March 2015
Received in revised form 15 April 2015
Accepted 13 May 2015
Available online 19 May 2015

Keywords:
biomass
activated carbon
electrode material
electric double-layer capacitors (EDLCs)

ABSTRACT

Activated carbons (ACs) are successfully synthesized from corncob by a simple chemical activation methodology and demonstrated as novel, suitable electrode materials for electric double-layer capacitors (EDLCs). The as-prepared samples were characterized by SEM, TEM, XPS, FT-IR and N_2-sorption followed by further electrochemical characterization. All samples exhibit a high specific surface area, favorable pore size distribution combining good electrical conductivity and excellent capacitive performance. The optimal sample achieved not only high specific capacitance (401.6 F g^{-1} in 0.5 M H_2SO_4 and 328.4 F g^{-1} in 6 M KOH aqueous electrolyte at a current density of 0.5 A g^{-1}), but also showed excellent cycling performance, with 100% and ~91% retention over 10000 cycles at 5 A g^{-1} in the above mentioned electrolytes. Furthermore, the sample also displayed improved rate capability with discharge capacitance retention of ~60% at 20 A g^{-1} in 0.5 M H_2SO_4 and ~75% at 20 A g^{-1} in 6 M KOH. The results indicate surface functional groups associate with high surface area and appropriate microstructure affect the capacitive performance of corncob-based ACs significantly. Herein, ACs prepared from corncobs are presented as a promising substitute to conventional electrode materials for EDLCs.

1. Introduction

Supercapacitors can bridge the gap between conventional capacitors and rechargeable batteries. As one of the most promising electrochemical energy storage systems, supercapacitors along with lithium-ion battery have attracted much attention due to their wide applications ranging from mobile devices to electric vehicles. Normally, supercapacitors serve as auxiliary power source in electric vehicles since it can offer high power density, however Li-ion battery cannot when the car is about to start and accelerate. Therefore, it is a matter of considerable interest to improve energy density and reduce cost before large-scale industrial applications for supercapacitors.

Basically, there are two kinds of charge storage mechanisms in supercapacitors: double layer capacitance effects – with carbon electrodes or derivates with predominant electrostatic double-layer capacitance and pseudo-capacitance effects – with metal oxide or conducting polymer electrodes with a high amount of electrochemical pseudo-capacitance. Despite the fact that pseudo-capacitors have relatively high energy densitiy due to the introduction of redox reactions, disadvantages such as inferior cycling stabilities and high cost are barriers to their commercialization. Conversely, EDLCs have advantages like good cycling stabilities, high rate performance, and high power density and disadvantages such as limited energy densities. High surface areas, optimized pore structures, and favorite surface functional groups of the electrode materials have been suggested to be the key issues in improving electrode performance in EDLCs [1–4]. Accordingly, numerous carbon-based materials such as activated carbons (ACs) [5], activated graphene [6], carbon nanotubes [7] and carbon aerogels [8] and the like have been subjected to intensive research in the past decades.

Among the aforementioned carbon materials, activated carbons derived from agricultural wastes (such as corn stover [9], coconut shells [10], coffee beans [11] and cotton stalk [12]) gathered much attention due to their low cost, easy accessibility, non-toxicity and good chemical stability, and turned out to be the most promising candidates for future energy storage. Additionally, activated carbons derived from agricultural wastes tend to be rich in nitrogen and oxygen functional groups [13,14], which are favorable to enhance the capacity. In this paper, activated carbons derived from corncobs are prepared by simple chemical activation process

* Corresponding author. Tel.: +86 21 69589355; Fax: +86 21 69589355.
E-mail address: zhangcunman@tongji.edu.cn (C. Zhang).

http://dx.doi.org/10.1016/j.electacta.2015.05.080
0013-4686/

and then employed as electrode materials for EDLCs. The as-obtained samples delivered high capacitance and excellent cycling performance in aqueous electrolytes with well-developed microporosity (specific surface area up to 3054 $m^2 g^{-1}$, 49 vol% micropores). Effects of surface chemical properties on the capacitive performance in different aqueous electrolytes are also elaborated here.

2. Experimental

2.1. Synthesis of corncob-based activated carbons

Activated carbons were prepared by the following strategies: (i) pyrolysis/carbonization of corncobs and (ii) chemical activation with KOH as activating agent. Detailed processes were given in our previous report [15]. An additional ball milling process was introduced after activation to obtain finer powders that favored for electrode fabrication. The as-obtained samples are hereafter designated as "Cxxx", xxx is the activation temperature of samples (Table 1).

2.2. Characterization

The scanning electron microscopy (SEM, FEI SIRION 200/INCA, OXFORD) and transmission electron microscopy (TEM, JEM-2100F, JEOL) were used to determine the morphology and texture of the samples. Elemental analysis (Elementar, vario EL III), X-ray photoelectron spectroscopy (XPS, UlVAC-PHI PHI 5000 VersaProbe) and Fourier Transform Infrared Spectrometer (FT-IR, BRUKER, EQUINOXSS/HYPERION 2000) were employed to determine the element content and surface functional groups. A high accuracy balance (METTLER TOLEDO with 0.00001 g accuracy) was used to diminish the experimental error.

Nitrogen sorption isotherms and textural properties of all samples were determined at −196 °C using nitrogen in a conventional volumetric technique by a Micromeritics ASAP 2020 sorptometer over a wide relative pressure range from about 10^{-6} to 0.995. The surface area was calculated using the Brunauer–Emmett–Teller (BET) equation based on adsorption data in the partial pressure (P/P_0) ranging from 0.02 to 0.25 and the total pore volume was determined from the amount of nitrogen adsorbed at a relative pressure of 0.98. Pore size distributions (PSDs) were calculated by using the Density Functional Theory (DFT) Plus Software (provided by Micromeritics Instrument Corporation), which is based on calculated adsorption isotherms for pores of different sizes. All of the samples were degassed at 300 °C for 600 min prior to the measurements.

2.3. Electrochemical measurements

Electrochemical measurements for different as-prepared samples along with the commercial activated carbon (NORIT® A SUPRA) which was ordered from Sigma–Aldrich and used as reference materials in this work, were carried out in a three-electrode system: The working electrode was prepared by mixing 80 wt.% active material, 15 wt.% Super-P carbon black and 5 wt.% polytetrafluoroethylene (PTFE) binder in de-ionized water. The slurry of the mixture was dried at 80 °C for two hours and then rolled into sheet and pressed onto the nickel foam under a pressure of 10 MPa. The mass loading of the active materials is about 2∼4 mg. A platinum plate electrode served as counter electrode and an Hg/HgO or Ag/AgCl electrode served as reference electrode in 6 M KOH or 0.5 M H_2SO_4 aqueous electrolyte, respectively. Electrochemical performance was measured at room temperature.

Symmetric supercapacitor was also fabricated to investigate the practical performance of the samples. In two-electrode system measurements, the preparation process of the electrodes were almost the same with three-electrode system except that circular electrodes were employed to match the testing configuration. The cathode and anode electrodes were pressed together and separated by polypropylene membrane. The electrochemical measurements of the symmetric supercapacitor were carried out in both alkaline and acidic electrolytes using the electrochemical working station in a two-electrode cell at room temperature.

Cyclic voltammetry (CV) was carried out by six repeated cycles at a scan rate ranging from 5 to 100 mV s^{-1}. Galvanostatic charge/discharge (GCD) was tested at a current density load ranging from 0.5 to 20 A g^{-1} and electrochemical impedance spectroscopy (EIS, frequency ranging from 0.1 Hz to 100,000 Hz with potential amplitude of 10 mV) was performed on a CHI 760E electrochemical workstation.

3. Results and discussion

Fig. 1 shows the SEM and TEM images of a typical as-prepared sample-C850 (The SEM and TEM images of sample C650 and C750 are not shown here since they are similar with C850). It mainly composed of vast irregular granules which results from the introduction of ball milling process after activation, and demonstrates uniform pore size distribution which confirmed the well-developed microporosity of the sample. Apparently, finer granularity and well-developed microstructure may be favorable to fast charge transfer and large charge storage capacity, and this will be discussed later.

The N_2-sorption isotherms and pore size distributions (PSDs) of all samples are schematically shown in Fig. 2. The isotherm of samples C650, C750, C850 and Norit A Supra belong to typical type I according to the IUPAC classification, a characteristic of microporous materials. The PSDs of all samples are similar, ranging from 0.5 nm to 4 nm. Combined with the morphology and microstructure demonstrated in Fig. 1, the hierarchical microstructure is concluded since the sample comprises certain external pores and great amount of internal micro- as well as meso-pores in the carbon granules. It has been proved that the micropores between 0.8 and 1.4 nm, would be fully accessible to the hydronium ions (0.36–0.42 nm) [16], and hydrated bisulfate ions (0.53 nm) [17,18] produced by dissociation of the electrolyte (0.5 M H_2SO_4), which indicates that the methodology in this paper is favorable for massively producing ACs for electrochemical energy storage.

Normally, carbons derived from biomass materials mainly consist of organics are rich in nitrogen and oxygen functional groups [14,19]. However, the as-prepared samples derived from corncobs are rich in oxygen contents (as high as 14.53%) but have

Table 1
Different Prepared Conditions for Different Corncob Activated Carbon Samples.

Sample	Heating Rate	Activation Temperature	Activation Time	Ball Milling Time	KOH/Carbon Ratio	Yield
C650	5 °C /min	650 °C	3 h	120 min	4	45.2%
C750	5 °C /min	750 °C	3 h	120 min	4	38.6%
C850	5 °C /min	850 °C	3 h	120 min	4	27.5%
Norit A Supra	Commercial activated carbon					

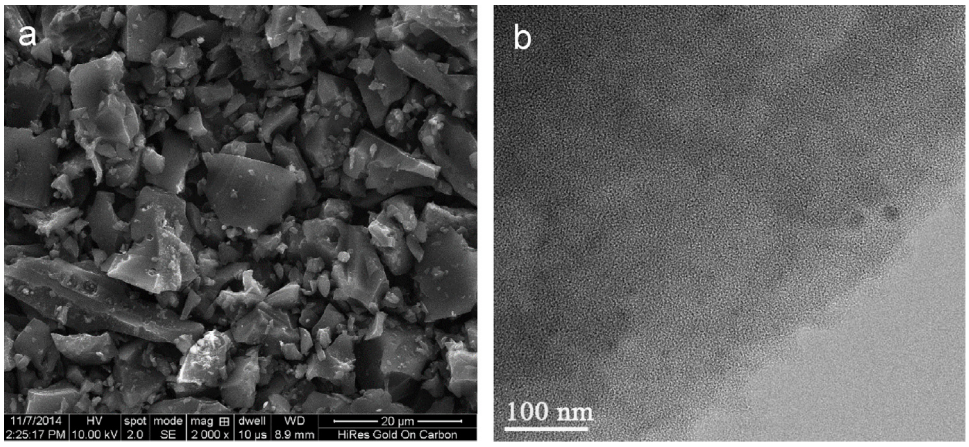

Fig. 1. Typical (a) SEM and (b) TEM images of the corncob-based activated carbon prepared at 850 °C.

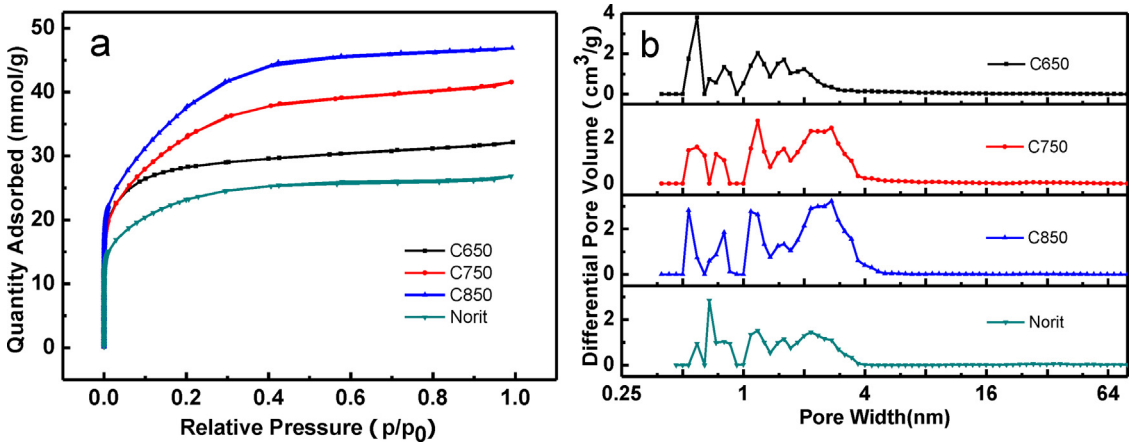

Fig. 2. (a) N_2-sorption isotherms and (b) pore size distributions of different samples.

Table 2
Textural Parameters Deduced from N_2 Adsorption and Elemental Composition of different samples.

Sample	S_{BET} (m^2g^{-1})	V_t (cm^3g^{-1})	Pore volume (cm^3g^{-1}) by DFT method(nm)				Chemical composition (at %)		
			V_2 (<1)	V_3 (1- 2)	V_4 (2 -5)	V_5 (>5)	C	O	N
C650	2380	1.10	0.352	0.411	0.123	0.216	83.64	14.53	<0.3
C750	2701	1.42	0.236	0.447	0.484	0.253	88.20	10.44	0.75
C850	3054	1.50	0.246	0.492	0.651	0.111	89.45	9.49	<0.3
Norit	1899	0.91	0.220	0.319	0.222	0.149	89.00	9.64	<0.3

few nitrogen heteroatoms (less than 1%) according to the elemental analysis results in Table 2. Fig. 3 presents the X-ray photoelectron spectroscopy (XPS) of different samples, which was used to evaluate the surface chemical properties of the as-prepared samples. The XPS spectra of the O1s region can be approximately fitted into four main peaks corresponding to oxygen atoms in C=O groups (BE≈531.5 eV) [20], oxygen atoms in C-O groups in C-OH and/or COOR (BE≈532.0-532.1 eV) [21], oxygen in C-OH/C-O-C groups (BE≈532.7-533.0 eV) [22] and oxygen in –OH groups (BE≈533.4 eV) [23]. It is widely accepted that the oxygen functionalities on carbons contribute to the pseudo-capacitance through the quinone/hydroquinone redox pair [24,25]. Furthermore, Fourier transform infrared (FT-IR) spectroscopy was used to verify the existence of the aforementioned functionalities in Fig. 4. Basically, the spectrum displays five broad bands, which may result from the overlap of the adsorption of many similar functional groups. The most prominent adsorption band at 1060–1095 cm^{-1} (D) should belong to the C-O stretching vibration of various functionalities [26]. Other bands at 2350 cm^{-1} (A), 1545 cm^{-1} (C) and 800 cm^{-1} (E) possibly originate from hydrogen bonded or ionized compound structure [27], highly conjugated C–O in a quinone/carbonyl structure [28] and C-H (alkenes) [29]. The presence of carboxylic functionalities were shown by the band at 1680–1720 cm^{-1} (B), which caused by COOH vibrations [30]. The existence of the carboxylic groups can further improve the wettability of the carbon surface and reduce the charge transfer resistance, which are beneficial to the improvement of the electrochemical performance of ACs [13].

Electrochemical performance in both alkaline and acidic media were characterized in this study. A commercial activated carbon (NORIT® A SUPRA) with a specific surface area of 1899 $m^2 g^{-1}$ was also tested as a reference. Galvanostatic charge/discharge (GCD) curves of the C650, C750, C850 and Norit A Supra electrodes at a constant current density of 0.5 A g^{-1} in different electrolytes are

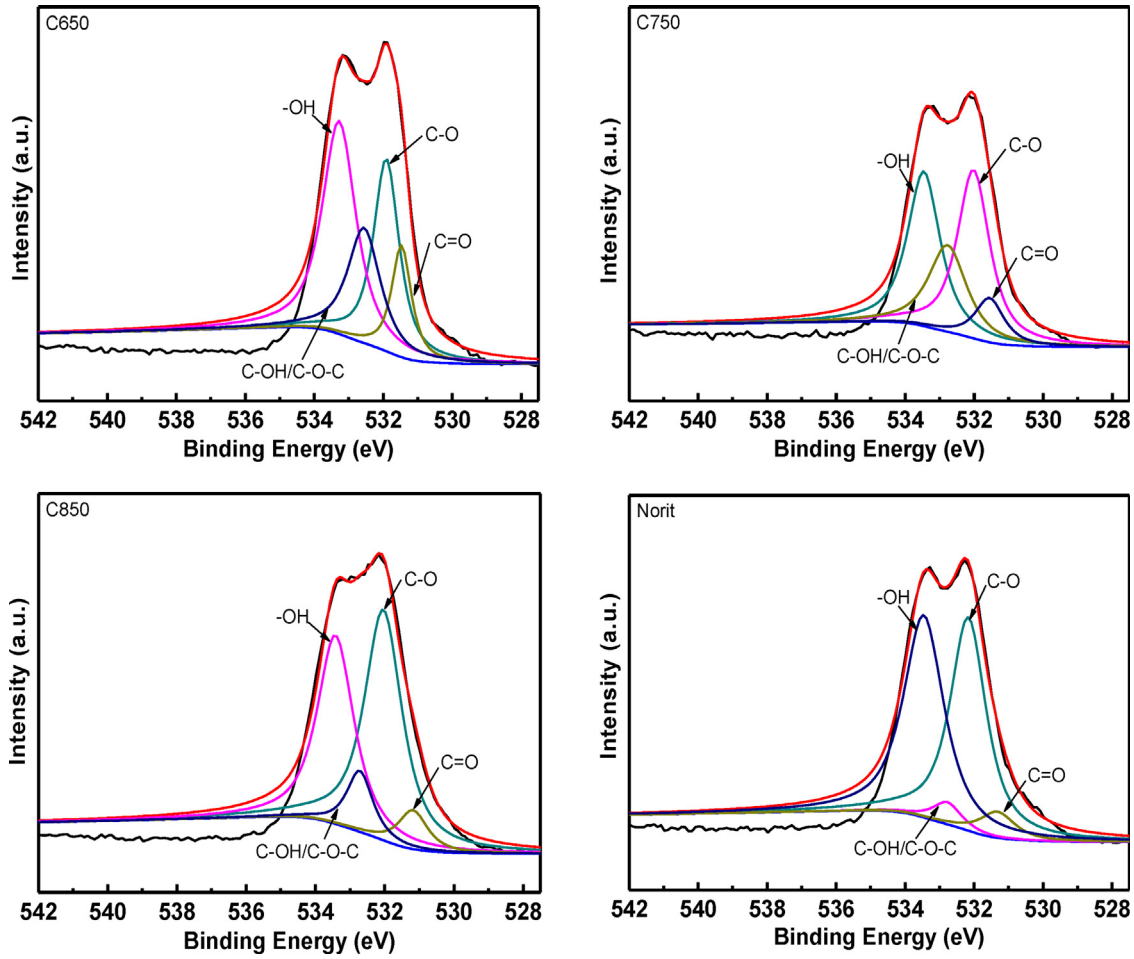

Fig. 3. XPS spectra of the O1s region for different samples.

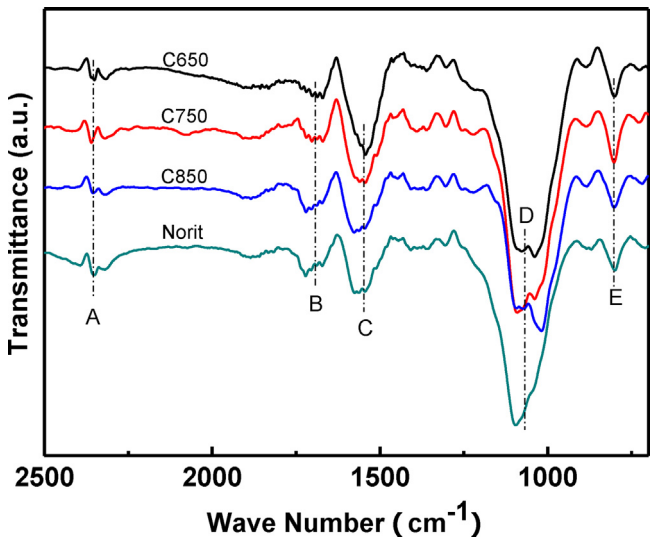

Fig. 4. FT-IR spectra of different samples.

given in Fig. 5a and b, and none of the samples demonstrate significant IR drops, indicating good electrical conductivity. Typical symmetric triangle-shaped curves are observed in both alkaline and acidic electrolytes, which indicate the dominated double layer charge storage effects. As depicted in Fig. 5c and d, even at high current density, the GCD curves of the as-prepared samples remain nondeflecting and show tolerable IR drops (~0.1 V at current density as high as 20 A g^{-1}). Meanwhile, a slight distortion of the GCD curves measured in H_2SO_4 electrolyte reveals the existence of pseudo-capacitance arises from the reversible reduction/oxidation reactions of the surface functional groups. This can be also attested by the cyclic voltammetry (CV) curves at a sweep rate of 5 mV s^{-1} in Fig. 5e and f. Curves exhibit a quasi-rectangular shape, demonstrating the characteristic of an electrical double-layer capacitance with fast charge/discharge processes in Fig. 5e. The rectangular-like shape and the appearance of apparent humps imply the capacitive response results from the combination of electric double-layer capacitance and pseudo-capacitance in Fig. 5f, which are in accordance with the results deduced from GCD curves. In addition, the CV curve of sample C650 displays a much distinct hump than the others as the sample has the largest proportion of heteroatoms as depicted in Table 2. It must be mentioned that the CV curves of C650 and C850 recorded in KOH electrolyte show an unexpected distortion at the potential of about −0.25 V which could be ascribed to the abnormality originated from the Hg/HgO reference electrode.

Fig. 5g shows the relationship between the current density and the specific capacitance of the samples. And Table 3 summaries the specific capacitance of all samples calculated from the GCD curves at current density ranging from 0.5 to 20.0 A g^{-1}. The specific capacitance of C850 can reach a maximum of 401.6 F g^{-1} in H_2SO_4 electrolyte and 328.4 F g^{-1} in KOH electrolyte at 0.5 A g^{-1}. Even at high current loading of 20 A g^{-1}, the sample maintained as high as 239.7 F g^{-1} in H_2SO_4 electrolyte and 245.6 F g^{-1} in KOH, both of

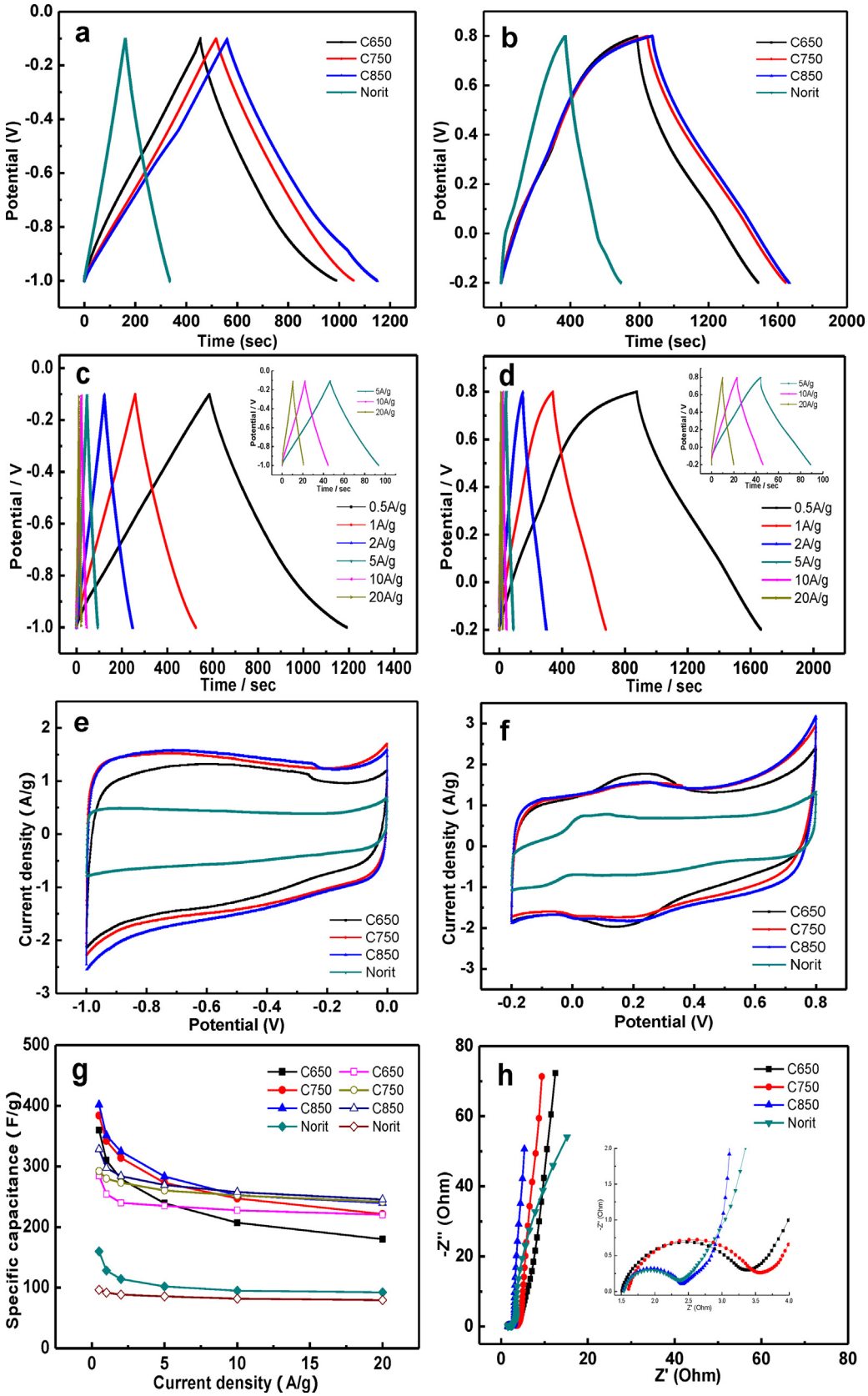

Fig. 5. GCD curves of different electrodes at a constant current density of 0.5 A g^{-1} in (a) 6 M KOH electrolyte and (b) 0.5 M H_2SO_4 electrolyte; GCD curves of the C850 electrode at various constant current density (0.5~20 A g^{-1}) in (c) 6 M KOH electrolyte and (d) 0.5 M H_2SO_4 electrolyte; CV curves of different electrodes at a scan rate of 5 mV s^{-1} (e) 6 M KOH electrolyte and (f) 0.5 M H_2SO_4 electrolyte; (g) Capacitance versus discharge current density from 0.5 A g^{-1} to 20 A g^{-1} comparing different electrodes (solid: 0.5 M H_2SO_4, open: 6 M KOH); (h) Nyquist plot of different electrodes in 0.5 M H_2SO_4 electrolyte over the frequency range from 0.01 Hz to 100 kHz.

Table 3
Comparison of the Electrochemical Performance of Different Samples in Three-electrode System.

electrolyte	Samples	Capacitance/F g^{-1}					
		0.5A g^{-1}	1A g^{-1}	2A g^{-1}	5A g^{-1}	10A g^{-1}	20A g^{-1}
0.5M H_2SO_4	C650	359.9	309.9	279.2	239.3	207.2	180.2
	C750	383.9	342.2	314.1	272.9	247.3	221.5
	C850	401.6	351.2	324.6	283.3	252.5	239.7
	Norit	160	128.5	114.3	102.1	95.2	92.6
6M KOH	C650	284.5	254.5	239.8	234.9	227.8	220.3
	C750	292.1	279.9	273.2	260.4	252.3	241.7
	C850	328.4	297.7	284.0	269.5	257.7	245.6
	Norit	96.6	91.8	88.6	85.8	82.1	79.6

which are much higher than that of Norit A Supra. This should be attributed to the considerable larger specific surface area, well-developed microstructures and ample favorable functionalities. The specific capacitance of 401.6 F g^{-1} at 0.5 A g^{-1} in 0.5 M H_2SO_4 is the highest among previously reported at similar testing conditions for ACs prepared from a wide variety of biomass precursors [14,31]. It is noticeable that all samples show much higher specific capacitance in acidic electrolyte than that in alkaline electrolyte due to the existence of partial pseudo-capacitance results from the presence of surface quinone groups. The enhanced capacitance involving pseudo-capacitance effects in acidic electrolyte also drops quickly with the increase of current density. This should be induced by the incomplete electrochemical reactions concerning the functionalities at high current density. In addition, although the amount of surface functionalities of C650 precedes that of C750 and C850, the superiority can be offset by the scarcity of large specific surface area and lower electronic conductivity. The outstanding electrochemical performance of the as-prepared ACs highlights the significance of the integration of the high surface area with ample microporosity and surface functionalities.

The electrochemical impedance spectroscopy (EIS) was conducted to investigate the electrochemical properties of the as-prepared ACs as electrode materials in Fig. 5h. A combination of semicircle in the middle and high frequency and a linear region in the low frequency was observed in both of these Nyquist plots. Normally, the first intersection point on the real axis is termed the equivalent series resistance (ESR), which relates to three kinds of resistance: the resistance of the electrolyte, the intrinsic resistance of the active material and the interfacial contact resistance of the active material/current collector [32,33]. As is shown in Fig. 5h, the ESR of C850 and Norit A Supra are about 0.8 Ω, and the ESR of C650 and C750 are about 1.8∼1.9 Ω. Namely, the sample prepared at higher temperature is favorable for fabricating materials for electrochemical energy storage since incomplete reorganization of carbon skeleton at lower activation temperature would result in poor electronic conductivity, which impedes the application of ACs in practical situations. Moreover, an almost vertical line is observed in the low-frequency region, which indicates a good capacitive performance of the as-prepared ACs.

The cycling performance of the C850 electrode was also evaluated by GCD at a current density of 5 A g^{-1} in both acidic and alkaline aqueous electrolyte in Fig. 6. As demonstrated in Fig. 6a and b, the sample shows wonderful cycling performance with ∼91% retention over 10000 cycles at 5 A g^{-1} in 6 M KOH electrolyte and with no decay after 10000 cycles at 5 A g^{-1} in 0.5 M H_2SO_4 electrolyte, respectively, indicating that the charge/discharge process of the electrode is highly reversible. Interestingly, the cycling performance in acidic and alkaline aqueous electrolyte

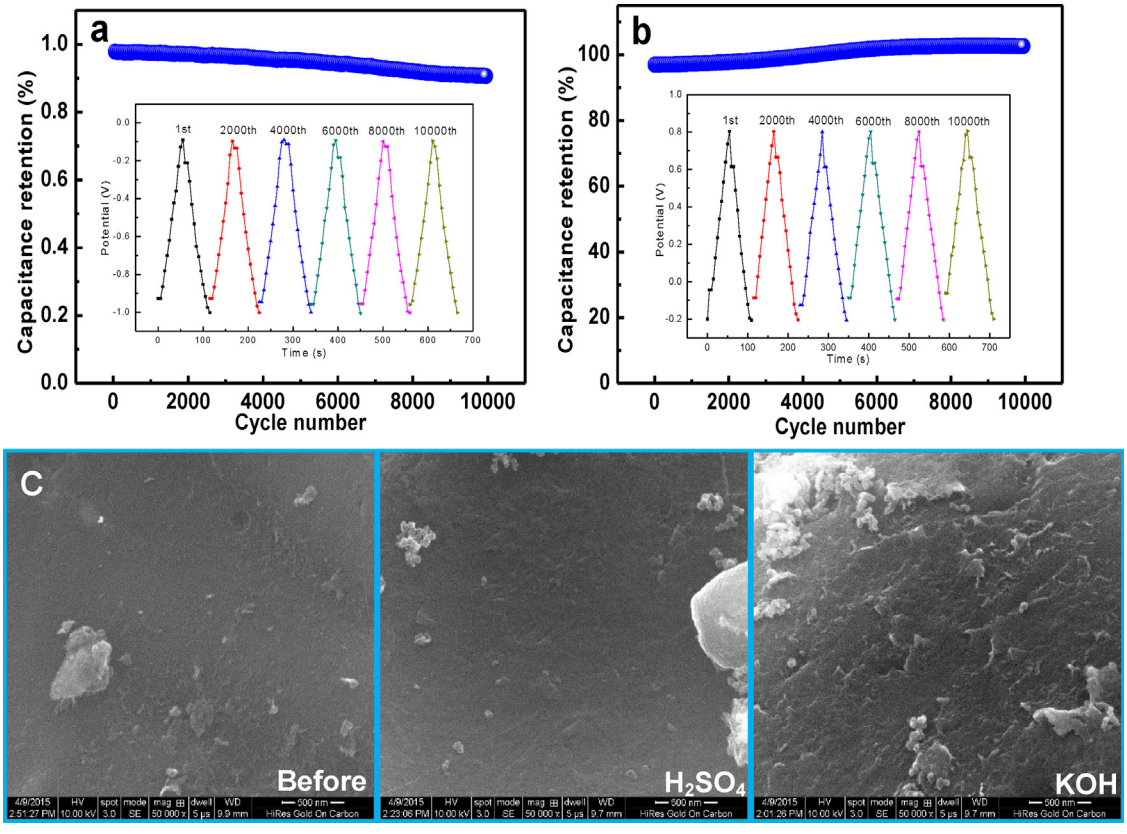

Fig. 6. Cycling performance of the C850 electrode at a current density of 5 A g^{-1} in (a) 6 M KOH electrolyte and (b) 0.5 M H_2SO_4 electrolyte; (c) SEM figures (50000x magnification, scale bar: 500 nm) of the C850 electrode before and after cycling performance measurements (from left to right: before cycling test, after cycling test in 0.5 M H_2SO_4, after cycling test in 6 M KOH).

displays totally opposite tendency. In acidic electrolyte, the samples are highly stable and the capacitance increases with micropores gradually infiltrated by electrolyte until all accessible micropores are fully activated. However, concentrated alkaline electrolyte tends to corrode the carbon skeleton and leads to the decreasing capacitance. This could also be validated by the SEM figures of the electrode before and after cycling performance measurements in Fig. 6c. As expected, the surface of the electrode tested in KOH electrolyte suffered a greater corrosion than that in H_2SO_4 electrolyte after 10000 cycles.

From the viewpoint of practical applications, we further investigated the performance of all samples in the symmetrical two-electrode system. As presented in Fig. 7, the almost symmetrical triangular GCD curves at various current density and the quasi-rectangular CV curves as well as typical EIS curves are observed, which are unique for double layer supercapacitors. Impressively, the specific capacitance of C850 in the two-electrode system (263.8 F g^{-1} at 0.5 A g^{-1} in 0.5 M H_2SO_4 electrolyte) is still remarkable and comparable to that of many other high-performance activated carbon materials derived from biomass precursors, such as activated carbon derived from sucrose (160 F g^{-1} at 0.1 A g^{-1}) [34], carbon obtained from cherry stones (230 F g^{-1} at 1 mA cm^{-2}) [35], based on the same electrolyte and similar testing conditions. For comparison, the performance of commercial activated carbon was also investigated in the symmetrical two-electrode system under the same conditions, and the results were collected in Table 4.

Table 4
Comparison of the Electrochemical Performance of Different Samples in Two-electrode System.

electrolyte	Samples	Capacitance/F g^{-1}			
		0.5A g^{-1}	1A g^{-1}	2A g^{-1}	5A g^{-1}
0.5M H_2SO_4	C650	217.6	202.4	186.2	160.4
	C750	242.4	224.4	208.3	185.2
	C850	263.8	247.2	230.2	205
	Norit	154.8	148	135.7	120.8
6M KOH	C650	162.6	158.4	153.5	142.6
	C750	179.4	174	167.2	150.4
	C850	194	185.6	183.3	170.2
	Norit	115.2	114	111.6	105.8

Based on the above results, the outstanding electrochemical performance of the as-prepared corncob-based activated carbons may arise from the following aspects. Firstly, high specific surface area along with ample microporosity is favorable for improving the effective contact area of electrode/electrolyte interface. Secondly, the hierarchical microstructure can facilitate the penetration of electrolytic ions, which results in excellent cycling stability and good rate capability. What is more, a great variety of surface functional groups can improve the wettability and electrical conductivity of the sample, thereby ensure the high performance of the electrode. In brief, high specific surface area and favorable microporosity along with hierarchical microstructure and ample surface functionalities synergistically result in the excellent electrochemical performance.

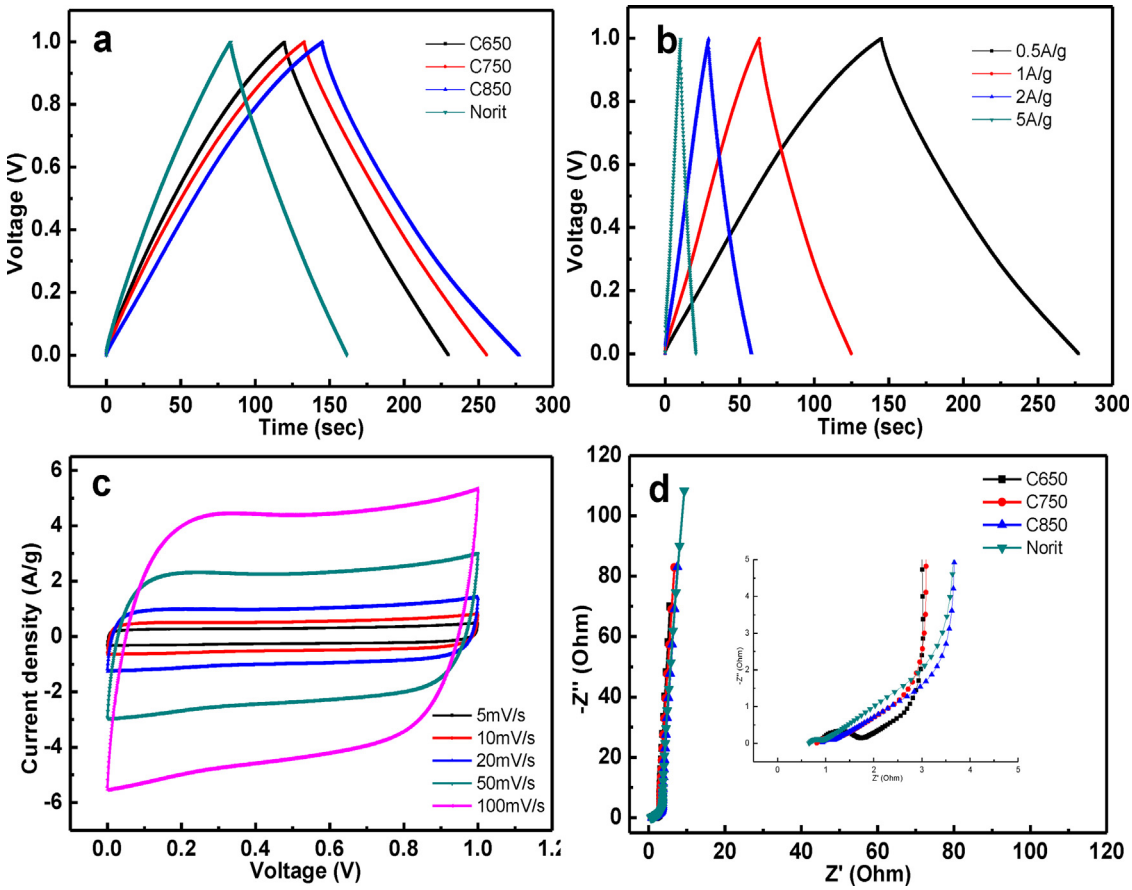

Fig. 7. Electrochemical performance in 0.5 M H_2SO_4 electrolyte based on the two-electrode system: (a) GCD curves of different capacitors at a constant current density of 0.5 A g^{-1} (based on the total active mass of both electrodes); (b) GCD curves of C850 capacitor at various current density and (c) CV curves of C850 capacitor at different scan rate; (d) Nyquist plot of different capacitors over the frequency range from 0.01 Hz to 100 kHz.

4. Conclusion

In summary, the as-obtained ACs from corncobs were prepared by a simple methodology and used for electrode materials for EDLCs. Synthesis parameters, such as activated temperature, were found to significantly affect the performance of the electrode materials. Sample prepared at 850 °C showed excellent performance as electrode material for EDLCs due to the synergistic effects of favorable surface functional groups and high specific surface area with well-developed microporosity as well as good electronic conductivity. The C850 achieved the highest specific capacitance of 401.6 $F g^{-1}$ in 0.5 M H_2SO_4 and 328.4 $F g^{-1}$ in 6 M KOH aqueous electrolyte at a current density of 0.5 $A g^{-1}$, respectively, with an excellent cycle life. With the results presented here, the as-obtained material is showed as highly active and durable electrode material for potential replacement of the conventional electrode materials for EDLCs.

Acknowledgments

This work was supported by the National High Technology Research and Development Program of China (863 Program) (2012AA053305, 2014AA052501).

References

[1] Z. Yu, L. Tetard, L. Zhai, J. Thomas, Supercapacitor electrode materials: nanostructures from 0 to 3 dimensions, Energy & Environmental Science (2014) .
[2] H. Itoi, H. Nishihara, T. Kogure, T. Kyotani, Three-dimensionally arrayed and mutually connected 1.2-nm nanopores for high-performance electric double layer capacitor, Journal of the American Chemical Society 133 (2011) 1165.
[3] Y. Korenblit, M. Rose, E. Kockrick, L. Borchardt, A. Kvit, S. Kaskel, G. Yushin, High-rate electrochemical capacitors based on ordered mesoporous silicon carbide-derived carbon, ACS Nano 4 (2010) 1337.
[4] L. Lai, H. Yang, L. Wang, B.K. Teh, J. Zhong, H. Chou, L. Chen, W. Chen, Z. Shen, R. S. Ruoff, Preparation of supercapacitor electrodes through selection of graphene surface functionalities, ACS nano 6 (2012) 5941.
[5] B. Xu, Y. Chen, G. Wei, G. Cao, H. Zhang, Y. Yang, Activated carbon with high capacitance prepared by NaOH activation for supercapacitors, Materials Chemistry and Physics 124 (2010) 504.
[6] M.D. Stoller, S. Murali, N. Quarles, Y. Zhu, J.R. Potts, X. Zhu, H.W. Ha, R.S. Ruoff, Activated graphene as a cathode material for Li-ion hybrid supercapacitors, Physical chemistry chemical physics: PCCP 14 (2012) 3388.
[7] C. Guo, N. Li, L. Ji, Y. Li, X. Yang, Y. Lu, Y. Tu, N- and O-doped carbonaceous nanotubes from polypyrrole for potential application in high-performance capacitance, Journal of Power Sources 247 (2014) 660.
[8] X.-L. Wu, T. Wen, H.-L. Guo, S. Yang, X. Wang, A.-W. Xu, Biomass-derived sponge-like carbonaceous hydrogels and aerogels for supercapacitors, ACS nano 7 (2013) 3589.
[9] H. Jin, X. Wang, Y. Shen, Z. Gu, A high-performance carbon derived from corn stover via microwave and slow pyrolysis for supercapacitors, Journal of Analytical and Applied Pyrolysis (2014) .
[10] A. Jain, V. Aravindan, S. Jayaraman, P.S. Kumar, R. Balasubramanian, S. Ramakrishna, S. Madhavi, M.P. Srinivasan, Activated carbons derived from coconut shells as high energy density cathode material for Li-ion capacitors, Scientific reports 3 (2013) 3002.
[11] T.E. Rufford, D. Hulicova-Jurcakova, Z. Zhu, G.Q. Lu, Nanoporous carbon electrode from waste coffee beans for high performance supercapacitors, Electrochemistry Communications 10 (2008) 1594.
[12] M. Chen, X. Kang, T. Wumaier, J. Dou, B. Gao, Y. Han, G. Xu, Z. Liu, L. Zhang, Preparation of activated carbon from cotton stalk and its application in supercapacitor, Journal of Solid State Electrochemistry 17 (2012) 1005.
[13] L. Jiang, J. Yan, L. Hao, R. Xue, G. Sun, B. Yi, High rate performance activated carbons prepared from ginkgo shells for electrochemical supercapacitors, Carbon 56 (2013) 146.
[14] A. Elmouwahidi, Z. Zapata-Benabithe, F. Carrasco-Marin, C. Moreno-Castilla, Activated carbons from KOH-activation of argan (Argania spinosa) seed shells as supercapacitor electrodes, Bioresource technology 111 (2012) 185.
[15] C. Zhang, Z. Geng, M. Cai, J. Zhang, X. Liu, H. Xin, J. Ma, Microstructure regulation of super activated carbon from biomass source corncob with enhanced hydrogen uptake, International Journal of Hydrogen Energy 38 (2013) 9243.
[16] L. Eliad, G. Salitra, A. Soffer, D. Aurbach, Ion sieving effects in the electrical double layer of porous carbon electrodes: estimating effective ion size in electrolytic solutions, The Journal of Physical Chemistry B 105 (2001) 6880.
[17] M. Endo, T. Maeda, T. Takeda, Y. Kim, K. Koshiba, H. Hara, M. Dresselhaus, Capacitance and pore-size distribution in aqueous and nonaqueous electrolytes using various activated carbon electrodes, Journal of the Electrochemical Society 148 (2001) A910.
[18] C. Moreno-Castilla, M.B. Dawidziuk, F. Carrasco-Marín, E. Morallón, Electrochemical performance of carbon gels with variable surface chemistry and physics, Carbon 50 (2012) 3324.
[19] D. Hulicova-Jurcakova, M. Seredych, G.Q. Lu, T.J. Bandosz, Combined Effect of Nitrogen- and Oxygen-Containing Functional Groups of Microporous Activated Carbon on its Electrochemical Performance in Supercapacitors, Advanced Functional Materials 19 (2009) 438.
[20] M. Soria-Sánchez, A. Maroto-Valiente, J. Álvarez-Rodríguez, I. Rodríguez-Ramos, A. Guerrero-Ruíz, Efficient catalytic wet oxidation of phenol using iron acetylacetonate complexes anchored on carbon nanofibres, Carbon 47 (2009) 2095.
[21] B. Gao, P.S. Yap, T.M. Lim, T.-T. Lim, Adsorption-photocatalytic degradation of Acid Red 88 by supported TiO_2: Effect of activated carbon support and aqueous anions, Chemical Engineering Journal 171 (2011) 1098.
[22] Z. Li, Z. Xu, H. Wang, J. Ding, B. Zahiri, C.M.B. Holt, X. Tan, D. Mitlin, Colossal pseudo-capacitance in a high functionality–high surface area carbon anode doubles the energy of an asymmetric supercapacitor, Energy & Environmental Science 7 (2014) 1708.
[23] C.-M. Chen, Q. Zhang, M.-G. Yang, C.-H. Huang, Y.-G. Yang, M.-Z. Wang, Structural evolution during annealing of thermally reduced graphene nanosheets for application in supercapacitors, Carbon 50 (2012) 3572.
[24] E. Raymundo-Piñero, M. Cadek, F. Béguin, Tuning Carbon Materials for Supercapacitors by Direct Pyrolysis of Seaweeds, Advanced Functional Materials 19 (2009) 1032.
[25] E. Raymundo-Piñero, F. Leroux, F. Béguin, A High-Performance Carbon for Supercapacitors Obtained by Carbonization of a Seaweed Biopolymer, Advanced materials 18 (2006) 1877.
[26] A.-N.A. El-Hendawy, Surface and adsorptive properties of carbons prepared from biomass, Applied surface science 252 (2005) 287.
[27] X. Chen, S. Jeyaseelan, N. Graham, Physical and chemical properties study of the activated carbon made from sewage sludge, Waste Management 22 (2002) 755.
[28] C. Namasivayam, D. Kavitha, IR, XRD and SEM studies on the mechanism of adsorption of dyes and phenols by coir pith carbon from aqueous phase, Microchemical journal 82 (2006) 43.
[29] K. Foo, B. Hameed, Microwave assisted preparation of activated carbon from pomelo skin for the removal of anionic and cationic dyes, Chemical Engineering Journal 173 (2011) 385.
[30] I.A. Schepetkin, A.I. Khlebnikov, S.Y. Ah, S.B. Woo, C.-S. Jeong, O.N. Klubachuk, B.S. Kwon, Characterization and biological activities of humic substances from mumie, Journal of agricultural and food chemistry 51 (2003) 5245.
[31] Z. Li, Z. Xu, X. Tan, H. Wang, C.M.B. Holt, T. Stephenson, B.C. Olsen, D. Mitlin, Mesoporous nitrogen-rich carbons derived from protein for ultra-high capacity battery anodes and supercapacitors, Energy & Environmental Science 6 (2013) 871.
[32] M. Toupin, D. B¦langer, I.R. Hill, D. Quinn, Performance of experimental carbon blacks in aqueous supercapacitors, Journal of power sources 140 (2005) 203.
[33] K. Xie, X. Qin, X. Wang, Y. Wang, H. Tao, Q. Wu, L. Yang, Z. Hu, Carbon nanocages as supercapacitor electrode materials, Advanced materials 24 (2012) 347.
[34] L. Wei, G. Yushin, Electrical double layer capacitors with activated sucrose-derived carbon electrodes, Carbon 49 (2011) 4830.
[35] M. Olivares-Marín, J.A. Fernández, M.J. Lázaro, C. Fernández-González, A. Macías-García, V. Gómez-Serrano, F. Stoeckli, T.A. Centeno, Cherry stones as precursor of activated carbons for supercapacitors, Materials Chemistry and Physics 114 (2009) 323.